PHOTONICS Research

# Demonstration of electrically injected vertical-cavity surface-emitting lasers with post-supported high-contrast gratings

Jing Zhang,[1,2] Chenxi Hao,[1,2] Wanhua Zheng,[1,2,3] Dieter Bimberg,[4,5] and Anjin Liu[1,2,*]

[1]State Key Laboratory on Integrated Optoelectronics, Institute of Semiconductors, Chinese Academy of Sciences, Beijing 100083, China
[2]Center of Materials Science and Optoelectronics Engineering, University of Chinese Academy of Sciences, Beijing 100049, China
[3]Key Laboratory of Solid-State Optoelectronics Information Technology, Institute of Semiconductors, Chinese Academy of Sciences, Beijing 100083, China
[4]Bimberg Chinese-German Center for Green Photonics, Changchun Institute of Optics, Fine Mechanics and Physics, Chinese Academy of Sciences, Changchun 130033, China
[5]Institute of Solid State Physics and Center of Nanophotonics, Technische Universität Berlin, 10623 Berlin, Germany
*Corresponding author: liuanjin@semi.ac.cn

Received 4 November 2021; revised 17 January 2022; accepted 2 March 2022; posted 3 March 2022 (Doc. ID 447633); published 14 April 2022

**We experimentally demonstrate for the first time to our knowledge electrically injected vertical-cavity surface-emitting lasers (VCSELs) with post-supported high-contrast gratings (HCGs) at 940 nm. The HCG-VCSELs have two posts to support the air-suspended HCGs, which are realized by simple fabrication without critical point drying. The HCG-VCSEL achieves a threshold current of about 0.65 mA and a side-mode suppression ratio of 43.6 dB under continuous-wave operation at 25°C. Theoretically the HCG-VCSEL with a $\lambda/2$-cavity for the transverse magnetic polarization has a smaller effective mode length of $1.38 \cdot (\lambda/n)$. Thus, the relaxation resonance frequency can be increased by 16% compared with that of the conventional VCSEL. The modulation speed of 100 Gbit/s for the HCG-VCSEL is expected in the on–off keying modulation format. Our easy design of HCG-VCSELs has great potential for applications in optical interconnects, sensing, illumination, and so on.** 

https://doi.org/10.1364/PRJ.447633

## 1. INTRODUCTION

Applications of vertical-cavity surface-emitting lasers (VCSELs) are rapidly increasing. They are widely used for optical interconnects, mice, consumer electronics, 3D sensing like face recognition, or automotive applications. VCSELs have many unique features like circular beams, low power consumption, high modulation speed, low cost, high reliability, and easy fabrication of two-dimensional arrays [1–6]. The cavity of a VCSEL is composed of two distributed Bragg reflectors (DBRs). The DBRs show a polarization-insensitive high-reflectivity spectrum across a wide wavelength range, resulting from the constructive interference of the reflected waves from the interfaces between the high- and low-index layers. Twenty to 40 pairs of DBR layers with several micrometer thicknesses are needed to obtain high reflectivity, making the VCSEL bulky and leading to a high series resistance. Fabricating epitaxial DBRs in the blue-green or infrared wavelength ranges beyond 1.3 μm is complex.

High-contrast gratings (HCGs) show a near 100% reflectivity across a wide wavelength range and have a typical thickness of a few hundred nanometers, much thinner than that of epitaxial DBRs [7–12]. Thus, HCGs are ideal candidates for mirror replacements to construct vertical cavities. HCGs have been demonstrated to partly or fully replace DBRs to form HCG-DBR vertical cavities for VCSELs [13–24]. HCG-VCSELs have been attracting much attention since the first 850 nm GaAs-based HCG-VCSEL with single-mode operation and polarized output was demonstrated in 2007 [13]. Then GaAs-based HCG-VCSELs at 980 nm and 1060 nm wavelengths were realized with a large side-mode suppression ratio (SMSR) [17–20]. HCGs were also introduced to InP-based VCSELs to solve the technical challenge of p-type mirrors, and InP-based HCG-VCSELs working at 1320 and 1550 nm were demonstrated [15–17]. HCG-VCSELs at 1550 nm were proposed as light sources for silicon photonic circuits, and the HCG in the HCG-VCSEL works simultaneously as a mirror and a coupler [22,23]. Very recently, HCGs have been used in GaN-based VCSELs to replace the p-type mirror, and electrically injected GaN-based HCG-VCSELs at 400 nm were reported under pulsed conditions [24].

In the aforementioned HCG-VCSELs, HCGs are based often on an oxide layer, being monolithically integrated, or

air suspended. The fabrication of HCGs based on an oxide layer is difficult, because of the mismatched material systems [15,20,23–25]. Monolithic HCGs have a narrow high-reflectivity band and require tight fabrication tolerances [12,19]. Most HCGs are air suspended, leading to high index contrast and also wavelength tuning. The fabrication of air-suspended HCGs is again challenging. A carefully chosen sacrificial layer below the layer for defining the HCG pattern is required. Furthermore, critical point drying must be carefully done to avoid buckling of the grating, after the removal of the sacrificial layer [13,14,17,18,21].

Recently, standard design VCSELs at 940 nm have been attracting particular attention [5,6,26–31]. They are ideal laser sources for sensing. At 940 nm in comparison to 850 nm, the background from the sun is lower, the red glow becomes less visible, eye-safety margins are higher, and Si-CMOS is still sufficiently sensitive for detection; 940-nm VCSELs are also important for narrow-wave wavelength division multiplexing, and large progress in modulation speed and energy efficiency has been reported [29–31].

In this paper we report for the first time, to the best of our knowledge, post-supported HCG-VCSELs at 940 nm with an SMSR of 43.6 dB and a submilliamp threshold current. Our HCG-VCSELs incorporate air-suspended HCGs supported by two posts based on a simple fabrication technology without critical point drying. Furthermore, we propose a method to calculate the effective mode length to study the dynamical performance of HCG-VCSELs. Theoretically, the HCG-VCSELs have a smaller effective mode length, and they are expected to achieve a modulation speed of 100 Gbit/s in the on–off keying modulation format.

## 2. STRUCTURE AND DESIGN

The schematic of a 940 nm HCG-VCSEL is shown in Fig. 1(a). The structure is composed of a bottom semiconductor distributed Bragg reflector (DBR), a $\lambda$-cavity, and a top HCG-based reflector. The bottom DBR consists of n-doped 38.5-pair $Al_{0.12}Ga_{0.88}As/Al_{0.9}Ga_{0.1}As$ layers, leading to a high reflectivity of near 100%. The cavity consists of three InGaAs quantum wells surrounded by AlGaAs barriers. The photoluminescence spectrum has a peak at 926 nm and a full width at half-maximum of 17 nm. The top HCG-based reflector includes four-pair p-doped $Al_{0.12}Ga_{0.88}As/Al_{0.9}Ga_{0.1}As$ layers for current spreading and an air-suspended GaAs-based HCG, obtained after the removal of a lattice-matched GaInP sacrificial layer [32]. The GaAs-based HCG and the GaInP sacrificial layer are also p-doped. The GaInP sacrificial layer has the thickness of a three-quarter wavelength. The two posts to support the air-suspended HCG make it easy to release the HCG with a 100% yield without critical point drying in our experiments. The n and p contacts are formed at the back side of the substrate and on the top of the GaAs layer, respectively. The field distribution of the resonance mode is shown in Fig. 1(b). The confinement factor is about 2.7%.

The design of the GaAs-based HCG in Fig. 1(a) is based on a rigorous coupled wave analysis. The grating period is $\Lambda$, $a$ is the width of the grating bar, the duty cycle (DC) is defined as $a/\Lambda$, and $t_g$ is the thickness of the grating. The reflectivity

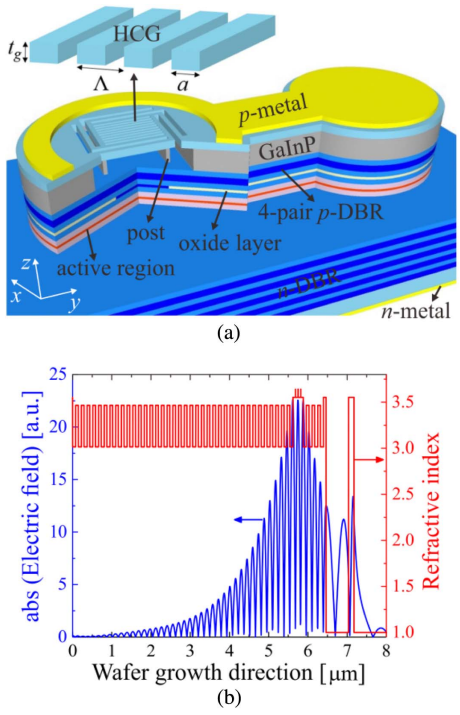


**Fig. 1.** (a) Schematics of the 940 nm HCG-VCSEL. The grating period is $\Lambda$, $a$ is the width of the grating bar, the duty cycle (DC) is defined as $a/\Lambda$, and $t_g$ is the thickness of the grating. (b) Field distribution of the resonance mode of our HCG-VCSELs.

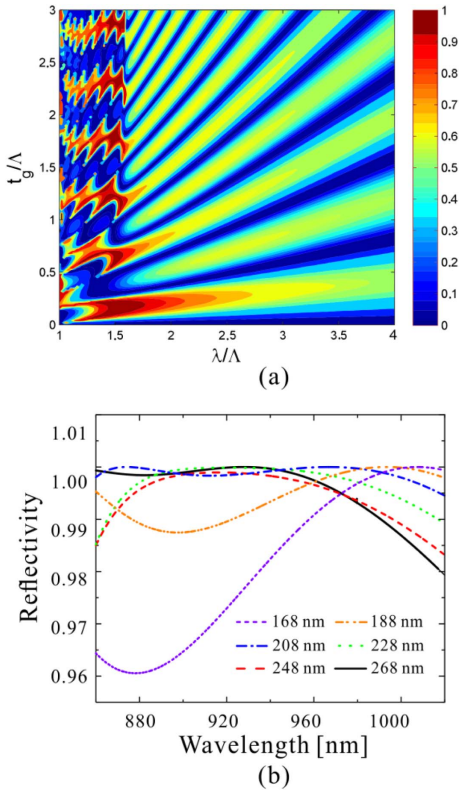


**Fig. 2.** (a) Reflectivity contour of the HCG as a function of normalized thickness ($t_g/\Lambda$) and normalized wavelength ($\lambda/\Lambda$) under normal incidence. (b) Reflectivity spectra of the HCGs for different bar widths for a grating period of 648 nm and a thickness of about a half wavelength.

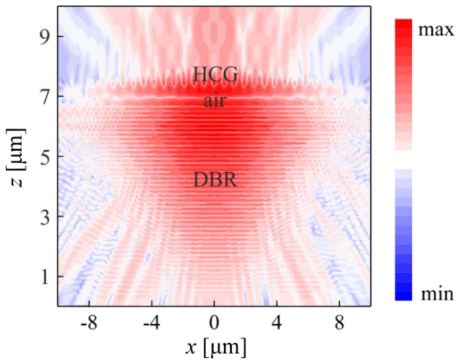


**Fig. 3.** Field distribution of the fundamental mode of the designed HCG-VCSEL with an oxide aperture of 4 μm in diameter. The resonant wavelength is 941.6 nm.

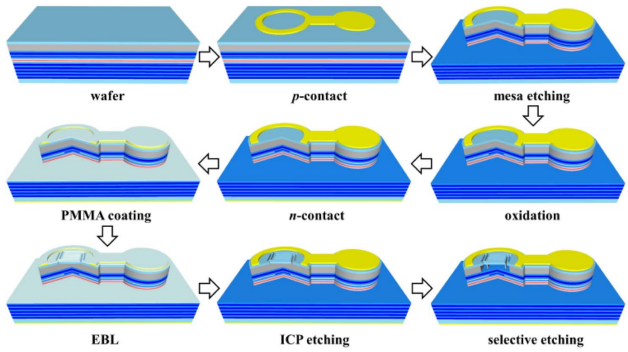


**Fig. 4.** Fabrication process flow of the HCG-VCSEL.

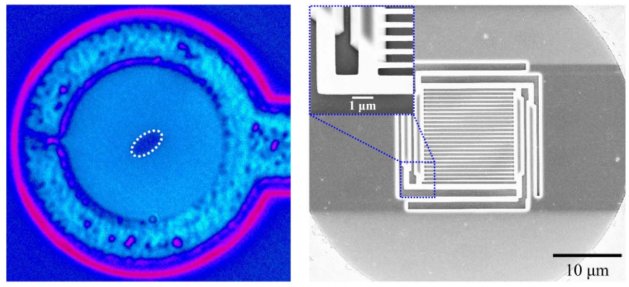


**Fig. 5.** (a) Infrared microscope image of the mesa after oxidation. The dashed ellipse indicates the profile of the oxidation edge. The size of the oxide aperture is about 4 μm × 8 μm. (b) SEM image of a typical air-suspended HCG with two posts of the HCG-VCSEL.

contour of the HCG is shown in Fig. 2(a) for the normalized wavelength ($\lambda/\Lambda$) and the normalized thickness ($t_g/\Lambda$) of the grating for transverse electric (TE, the electric field is parallel to the grating bar) polarization [27]. Figure 2(b) shows the reflectivity spectra of the HCGs for different bar widths (corresponding to duty cycles of from 26% to 41%) with a grating period of 648 nm and a thickness of about a half wavelength. The HCGs have high reflectivities (>99.5%) between 880 and 970 nm with the bar widths of 268, 248, 228, and 208 nm. When the bar widths are less than 208 nm, the reflectivities are less than 99.5% at 940 nm. However, the top four-pair $Al_{0.12}Ga_{0.88}As/Al_{0.9}Ga_{0.1}As$ DBR provides extra reflection, and the combination of the HCG with the four-pair DBR makes the top mirror achieve a reflectivity of larger than 99.5%.

The resonant modes of the designed HCG-VCSEL with an oxide aperture of 4 μm in diameter are simulated by the two-dimensional finite-difference time-domain method. The wavelength of the fundamental mode is 941.6 nm, and the quality ($Q$) factor is $1 \times 10^5$. The field distribution of the fundamental mode is shown in Fig. 3. The mode field is well confined in the vertical and horizontal directions.

## 3. FABRICATION

The epitaxial structure is grown on (100) GaAs substrates by metal-organic chemical vapor deposition (MOCVD). Subsequently, HCG-VCSELs are fabricated by standard VCSEL and HCG processing techniques [30,32]. Figure 4 schematically shows the fabrication process flow. First, the Ti/Pt/Au p contact is formed by a lift-off process. To form the mesa, the top GaAs layer is removed by the wet etching, and then the GaInP sacrificial layer is selectively etched. Next, an inductively coupled plasma (ICP) etching is used to etch the top $Al_{0.12}Ga_{0.88}As/Al_{0.9}Ga_{0.1}As$ DBR, active layers, and three pairs of the bottom DBR, to expose the 30 nm $Al_{0.98}Ga_{0.02}As$ layer. The $Al_{0.98}Ga_{0.02}As$ layer is then oxidized to form an oxide aperture in a water vapor atmosphere at 420°C with a home-built oxidation system. The Au/Ge/Ni/Au n contact is then deposited at the back side of the substrate and is annealed at 425°C.

To fabricate the HCG, poly(methyl methacrylate) (PMMA) electron resist is used for coating, and electron beam lithography (EBL, Raith 150 system) is used to define the subwavelength grating pattern. With the PMMA as a mask, the subwavelength grating pattern is transferred to the top GaAs layer by the ICP etching using a gas mixture of $BCl_3$ and Ar. Then the GaInP sacrificial layer is selectively removed by HCl. The wet etching rate of the GaInP sacrificial layer is anisotropic. Therefore, two posts beneath the HCG can be realized to support the air-suspended HCG without the critical point drying for the HCG release [32].

A number of mesas with diameters of from 70 to 90 μm are fabricated to form oxide apertures of different sizes. The oxidation aperture is checked by an infrared camera system after oxidation. An infrared microscope image of the oxidation aperture is shown in Fig. 5(a). Also, a series of HCGs with different duty cycles are defined for HCG-VCSELs. The scanning electron microscope (SEM) image of a typical air-suspended HCG with two posts is shown in Fig. 5(b).

## 4. EXPERIMENTAL RESULTS

The power-current-voltage ($L$-$I$-$V$) characteristics of the HCG-VCSELs are measured on wafer with a home-built probing system. The $L$-$I$-$V$ system is remote controlled and includes a source meter (Keithley 2401); a calibrated integrating sphere/photodetector system from Labsphere, Inc.; a thermoelectric cooler to control the temperature at 25°C; and a charge-coupled-device (CCD) camera. The fabricated HCG-VCSELs with a duty cycle of from 26% to 41% lase in our experiment.

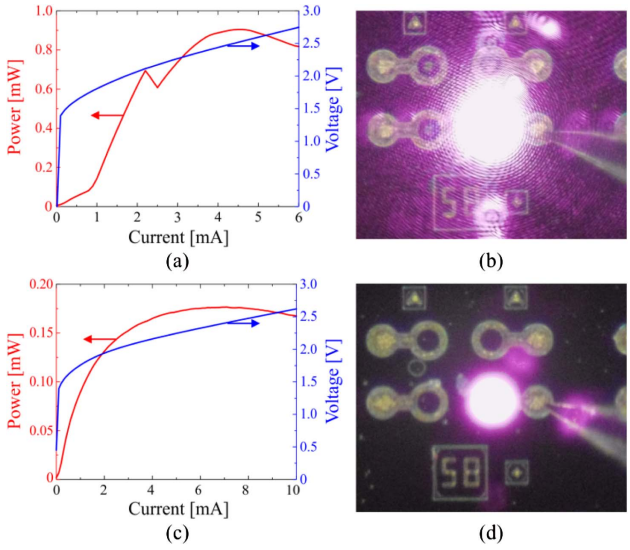


**Fig. 6.** (a) *L-I-V* curves of an HCG-VCSEL. (b) Lasing spot image from the CCD of the HCG-VCSEL at 2 mA. (c) *L-I-V* curves of the device without an HCG. (d) Image from the CCD of the devices without HCGs at 6 mA.

The continuous-wave (CW) *L-I-V* curves of the typical HCG-VCSEL with an HCG size of 10 μm × 10 μm are presented in Fig. 6(a). The threshold current $I_{th}$ is about 0.65 mA for this HCG-VCSEL. The threshold current can be reduced by reducing the oxide aperture and reasonably increasing the HCG size [33,34]. On the other hand, the electron beam lithography and ICP etching processes can be optimized for more perfect HCGs to reduce the extra losses. The *L-I* curve from 0 to 2 mA of the HCG-VCSEL in Fig. 6(a) is linear, and the HCG-VCSEL operates in single mode. The single-mode power at 2 mA is 0.63 mW. At higher currents than 2 mA, higher-order modes come out, with a kink in the *L-I* curve because of the thermal effect. To improve the single-mode output power in future experiments, the epitaxial structure of the HCG-VCSEL will be further optimized, and an optimized HCG with a larger size can be used.

Figure 6(b) shows the lasing spot image taken by a CCD at 2 mA, and the interference fringes are clearly visible. As designed, the air-suspended HCG here serves as a mirror with a high reflectivity, and a resonant cavity is formed, resulting in lasing. For comparison, the *L-I-V* characteristics of devices without HCGs are also measured. The devices without HCGs as shown in Fig. 6(c) do not lase. In Fig. 6(d), we can find no interference fringes in the image from the CCD for a device without an HCG at 6 mA.

Spectra of the HCG-VCSEL are measured under CW operation (AQ 6317B, resolution: 0.02 nm). As shown in Fig. 7(a), for the HCG-VCSEL with an oxide aperture of about 4 μm × 8 μm, the lasing wavelengths are around 946 nm. The HCG-VCSEL operates in single mode with an SMSR of 43.6 dB at 2 mA (about 3 × $I_{th}$). Spectra of the device without an HCG are measured at different currents and are shown in Fig. 7(b). They are broadband, confirming that the devices without HCGs operate as LEDs. The single-mode operation

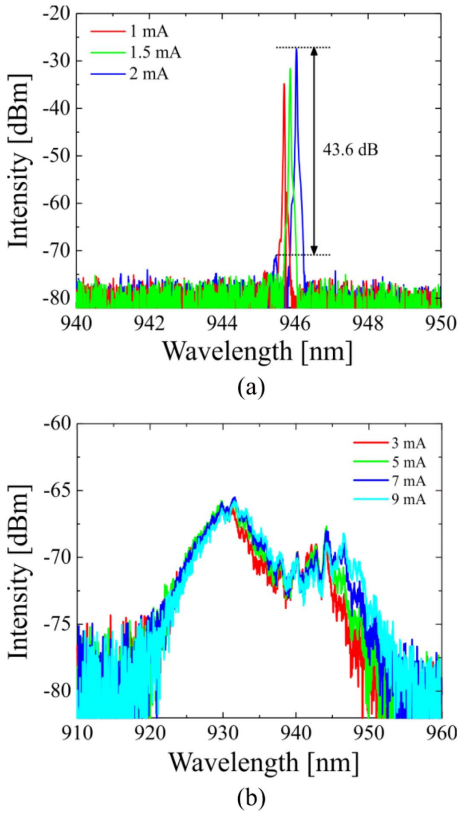


**Fig. 7.** (a) Spectra of the HCG-VCSEL under CW operation. (b) Spectra of the device without an HCG at different currents.

of the HCG-VCSEL is a result of the air-suspended HCG of the top reflector.

## 5. MODULATION PERFORMANCE ANALYSIS

The 940 nm HCG-VCSELs are candidates for narrow-wave wavelength-division multiplexing. HCGs were reported to have the ability to tightly confine the field in the HCG-based vertical cavities [35]. Experimentally, a −3 dB frequency of 27 GHz was obtained for an optically pumped hybrid vertical-cavity laser with lateral emission into a silicon waveguide [36]. This −3 dB bandwidth result of the HCG-VCSEL is less than the result of more than 30 dB of a conventional electrically injected VCSEL [3,22].

Here we propose a method to calculate the effective mode length and theoretically predict the modulation performance of the HCG-VCSEL. We expect to achieve a larger modulation bandwidth for HCG-VCSELs by optimizing the structure parameters, like the cavity length and the thickness of the sacrificial layer.

The relaxation resonance frequency $f_r$ of a VCSEL is expressed by [37]

$$f_r = \frac{1}{2\pi}\sqrt{\frac{\eta_i v_g}{qV_m}\times\frac{\partial g/\partial n}{\chi}(I - I_{th})}, \tag{1}$$

where $I_{th}$ is the threshold current, $\eta_i$ is the internal quantum efficiency, $v_g$ is the photon group velocity, $V_m$ is the mode

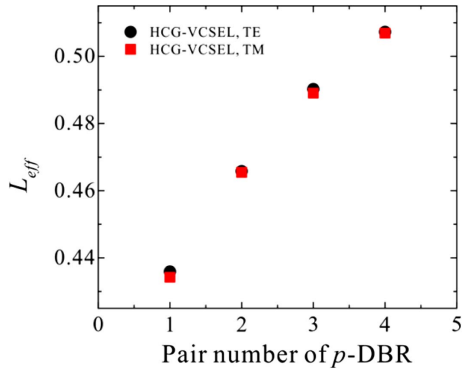


**Fig. 8.** Effective mode lengths of the HCG-VCSELs with different pair numbers of the p-DBR. The TM HCG has a grating period of 380 nm and a bar width of 230 nm. The thickness of the HCG is about a half wavelength.

volume, $\partial g/\partial n$ is the differential gain, and $\chi$ is the transport factor. Effective mode length $L_{\text{eff}}$ is used to characterize the mode confinement in VCSELs, and the mode volume $V_m$ is equal to the effective mode length $L_{\text{eff}}$ multiplied by the size of the active area. The effective mode length $L_{\text{eff}}$ is expressed by [38]

$$L_{\text{eff}} = \frac{\int n^2(z)E^2(z)\mathrm{d}z}{\max[n^2(z)E^2(z)]}, \tag{2}$$

where $n$ is the refractive index, $E$ is the electric field, and $z$ denotes the axis along the vertical direction as shown in Fig. 1(a).

The effective mode lengths of the HCG-VCSELs with different pair numbers of the p-DBR are shown in Fig. 8. The HCG-VCSELs have a $\lambda$-cavity and an air thickness of three-quarter wavelength beneath the HCG. The effective mode length is decreased as the pair number of the p-DBR is decreased. The TE HCG-VCSEL has a larger effective mode length than the TM (transverse magnetic, the electric field is perpendicular to the grating bar) HCG-VCSEL here, because there is higher field intensity in the TE HCG than that in the TM HCG of the HCG-VCSELs. For a reference, a conventional VCSEL with 23-pair top DBRs is used, and its epitaxial structure is the same as the HCG-VCSEL except for the p-DBR. The effective mode length $L_{\text{eff}-1}$ of the conventional VCSEL with a $\lambda$-cavity is 0.564 μm. The smallest effective mode length of the HCG-VCSEL in Fig. 8 is 0.434 μm ($0.77 \times L_{\text{eff}-1}$), and is $1.61 \times (\lambda/n)$, where $\lambda$ is 940 nm and $n$ is 3.5. The relaxation resonance frequency $f_r$ of the HCG-VCSEL is enhanced by about 14% compared with that of the conventional VCSEL with a $\lambda$-cavity, according to Eq. (1).

VCSELs with a $\lambda/2$-cavity can achieve a higher modulation bandwidth [3]. We further shorten the cavity length of the HCG-VCSEL from $\lambda$ to $\lambda/2$. At the same time, the air thickness beneath the HCG can be reduced from three-quarter wavelength to one-quarter wavelength for the TM polarization. The TM HCG-VCSEL with a $\lambda/2$-cavity and an air thickness of one-quarter wavelength beneath the HCG has an effective mode length of 0.372 μm. The effective mode length $L_{\text{eff}-0.5}$ of the conventional VCSEL with a $\lambda/2$-cavity is 0.498 μm.

**Table 1. Simulation Parameters for the TM HCG-VCSEL [37]**

| Parameter | Value |
|---|---|
| Confinement factor Γ | 0.065 |
| Cavity length (μm)[a] | 0.754 |
| Injection efficiency $\eta_i$ | 0.8 |
| Material gain coefficient $g$ ($\text{cm}^{-1}$) | 1800 |
| Nonlinear gain coefficient $\varepsilon$ ($\text{cm}^3$) | $1.5 \times 10^{-17}$ |
| Carrier density reduction $N_s$ ($\text{cm}^{-3}$) | $-0.4 \times 10^{18}$ |
| Carrier density at transparency $N_{\text{tr}}$ ($\text{cm}^{-3}$) | $1.8 \times 10^{18}$ |

[a]Calculated by the reflection phase [37].

Hence, the effective mode length of the HCG-VCSEL is $0.75 \times L_{\text{eff}-0.5}$, and is $1.38 \times (\lambda/n)$, where $\lambda$ is 940 nm and $n$ is 3.5. Therefore, the relaxation resonance frequency $f_r$ of the TM HCG-VCSEL is enhanced by 16% compared with that of the conventional VCSEL with a $\lambda/2$-cavity, according to Eq. (1).

The intrinsic modulation response of the HCG-VCSEL can be expressed by the transfer function [37]

$$H_i(f) = A \times \frac{f_r^2}{f_r^2 - f^2 + j\frac{f}{2\pi}\gamma}, \tag{3}$$

where $A$ is a constant, $j$ is the square root of −1, and $\gamma$ is the damping factor. The modulation response of the designed TM HCG-VCSEL with the parameters in Table 1 is shown in Fig. 9. The −3 dB frequency of the HCG-VCSEL can reach 46.8 GHz at 12 mA. This indicates that the 100 Gbit/s bit rate for the HCG-VCSEL is expected in the on–off keying modulation format, which is very promising for optical interconnects.

We propose the following approaches to achieve higher-speed operation of HCG-VCSEL than before. A TM HCG-VCSEL with a $\lambda/2$ cavity and an air thickness of one-quarter wavelength beneath the HCG is employed to reduce the effective mode length for large relaxation resonance frequencies. The number of the quantum wells is increased from 3 to 5, and the InGaAs quantum wells are optimized to increase the differential gain. Binary AlAs can be employed in the bottom DBR to improve the thermal conductivity

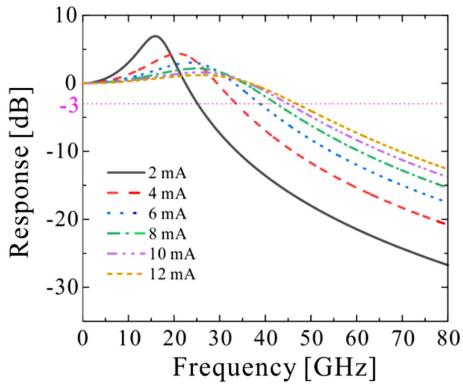


**Fig. 9.** Calculated small-signal modulation responses of the TM HCG-VCSEL with a $\lambda/2$-cavity and an air thickness of one-quarter wavelength beneath the HCG at different currents.

and reduce the thermal effect. Linearly graded DBRs with modulated doping can be used to lower the series resistance and reduce the loss. Two oxide apertures formed by selective wet oxidation of 30 nm thick $Al_{0.98}Ga_{0.02}As$ layers can be used for the transverse optical and current confinement. A double mesa structure can be used for a better heat dissipation, and bisbenzo-cyclobutene (BCB) planarization is used to lower the capacitance. Equalization, forward error correction, and electronic pulse shaping can be included with a wideband photodiode for high-speed transmission [39,40].

## 6. CONCLUSIONS

In conclusion, we reported for the first time to our knowledge electrically injected 940 nm HCG-VCSELs using post-supported air-suspended HCGs. Our current HCG-VCSEL can achieve a threshold current of about 0.65 mA and an SMSR of 43.6 dB at 25°C under CW operation. The HCG-VCSELs are fabricated without critical point drying, and the HCGs can be released with a 100% yield in water or isopropanol. The design and fabrication methods of the HCG-VCSELs can be extended to other wavelength ranges.

Theoretically, HCG-VCSELs can have smaller effective mode lengths compared with those of conventional VCSELs. A TM HCG-VCSEL with a $\lambda/2$-cavity and an air thickness of one-quarter wavelength beneath the HCG can achieve an effective mode length of $1.38 \times (\lambda/n)$. The −3 dB frequency of the HCG-VCSEL with a $\lambda/2$-cavity can theoretically reach 46.8 GHz at 12 mA, which indicates that 100 Gbit/s in the on–off keying modulation format for the HCG-VCSEL can be expected.

Our easy design of HCG-VCSELs has great potential for applications in optical interconnects, sensing, illumination, and so on. Next, the output power under single-mode operation of the HCG-VCSEL will be improved by optimizing the epitaxial structure, the size of the oxide aperture, and the HCG parameters. The dynamic performance of the optimized HCG-VCSEL will be studied. Also, the polarization and modulation characteristics will be studied, because these characteristics of VCSELs are important in applications like atomic sensing and 3D sensing.

**Funding.** National Natural Science Foundation of China (62075209, 61675193); Beijing Natural Science Foundation (Z200006).

**Disclosures.** The authors declare no conflicts of interest.

**Data Availability.** Data underlying the results presented in this paper are not publicly available at this time but may be obtained from the authors upon reasonable request.

## REFERENCES

1. F. Koyama, "Recent advances of VCSEL photonics," J. Lightwave Technol. **24**, 4502–4513 (2006).
2. R. Michalzik, *VCSELs—Fundamentals, Technology and Applications of Vertical-Cavity Surface-Emitting Lasers*, Springer Series in Optical Sciences (Springer, 2013), Vol. **166**.
3. A. Liu, P. Wolf, J. A. Lott, and D. Bimberg, "Vertical-cavity surface-emitting lasers for data communication and sensing," Photon. Res. **7**, 121–136 (2019).
4. A. Larsson, "Advances in VCSELs for communication and sensing," IEEE J. Sel. Top. Quantum Electron. **17**, 1552–1567 (2011).
5. H. Moench, S. Gronenborn, X. Gu, R. Gudde, M. Herper, J. Kolb, M. Miller, M. Smeets, and A. Weigl, "VCSELs in short-pulse operation for time-of-flight applications," Proc. SPIE **10938**, 109380E (2019).
6. L. A. Graham, H. Chen, J. Cruel, J. Guenter, B. Hawkins, B. Hawthorne, D. Q. Kelly, A. Melgar, M. Martinez, E. Shaw, and J. A. Tatum, "High power VCSEL arrays for consumer electronics," Proc. SPIE **9381**, 93810A (2015).
7. A. Liu, F. Fu, Y. Wang, B. Jiang, and W. Zheng, "Polarization-insensitive subwavelength grating reflector based on a semiconductor-insulator-metal structure," Opt. Express **20**, 14991–15000 (2012).
8. C. F. R. Mateus, M. C. Y. Huang, Y. Deng, A. R. Neureuther, and C. J. Chang-Hasnain, "Ultrabroadband mirror using low-index cladded subwavelength grating," IEEE Photon. Technol. Lett. **16**, 518–520 (2004).
9. A. Liu, W. Hofmann, and D. Bimberg, "2D analysis of finite size high-contrast gratings for applications in VCSELs," Opt. Express **22**, 11804–11811 (2014).
10. R. Magnusson and M. Shokooh-Saremi, "Physical basis for wideband resonant reflectors," Opt. Express **16**, 3456–3462 (2008).
11. P. Debernardi, R. Orta, T. Gründl, and M.-C. Amann, "3-D vectorial optical model for high-contrast grating vertical-cavity surface-emitting lasers," IEEE J. Quantum Electron. **49**, 137–145 (2013).
12. A. Liu, W. Zheng, and D. Bimberg, "Comparison between high- and zero-contrast gratings as VCSEL mirrors," Opt. Commun. **389**, 35–41 (2017).
13. M. C. Y. Huang, Y. Zhou, and C. J. Chang-Hasnain, "A surface-emitting laser incorporating a high-index-contrast subwavelength grating," Nat. Photonics **1**, 119–122 (2007).
14. M. C. Y. Huang, Y. Zhou, and C. J. Chang-Hasnain, "A nanoelectromechanical tunable laser," Nat. Photonics **2**, 180–184 (2008).
15. W. Hofmann, C. Chase, M. Müller, R. Yi, C. Grasse, G. Böhm, M. C. Amann, and C. J. Chang-Hasnain, "Long-wavelength high-contrast grating vertical-cavity surface-emitting laser," IEEE Photon. J. **2**, 415–422 (2010).
16. K. Li, Y. Rao, C. Chase, W. Yang, and C. J. Chang-Hasnain, "Monolithic high-contrast metastructure for beam-shaping VCSELs," Optica **5**, 10–13 (2018).
17. S. Boutami, B. Benbakir, J.-L. Leclercq, and P. Viktorovitch, "Compact and polarization controlled 1.55 μm vertical-cavity surface emitting laser using single-layer photonic crystal mirror," Appl. Phys. Lett. **91**, 071105 (2007).
18. E. Haglund, J. S. Gustavsson, J. Bengtsson, Å. Haglund, A. Larsson, D. Fattal, W. Sorin, and M. Tan, "Demonstration of post-growth wavelength setting of VCSELs using high-contrast gratings," Opt. Express **24**, 1999–2005 (2016).
19. M. Gębski, J. A. Lott, and T. Czyszanowski, "Electrically injected VCSEL with a composite DBR and MHCG reflector," Opt. Express **27**, 7139–7146 (2019).
20. S. Inoue, J. Kashino, A. Matsutani, H. Ohtsuki, T. Miyashita, and F. Koyama, "Highly angular dependent high-contrast grating mirror and its application for transverse-mode control of VCSELs," Jpn. J. Appl. Phys. **53**, 090306 (2014).
21. T. Ansbæk, I.-S. Chung, E. S. Semenova, and K. Yvind, "1060 nm tunable monolithic high index contrast subwavelength grating VCSEL," IEEE Photon. Technol. Lett. **25**, 365–367 (2013).
22. J. Ferrara, W. Yang, L. Zhu, P. Qiao, and C. J. Chang-Hasnain, "Heterogeneously integrated long-wavelength VCSEL using silicon high contrast grating on an SOI substrate," Opt. Express **23**, 2512–2523 (2015).
23. G. C. Park, W. Xue, A. Taghizadeh, E. Semenova, K. Yvind, J. Mørk, and I.-S. Chung, "Hybrid vertical-cavity laser with lateral emission into a silicon waveguide," Laser Photon. Rev. **9**, L11–L15 (2015).
24. T.-C. Chang, E. Hashemi, K.-B. Hong, J. Bengtsson, J. Gustavsson, Å. Haglund, and T.-C. Lu, "Electrically injected GaN-based vertical-cavity surface-emitting lasers with $TiO_2$ high-index-contrast grating reflectors," ACS Photon. **7**, 861–866 (2020).

25. A. Liu, B. Yang, P. Wolf, J. Zhang, and D. Bimberg, "GaAs-based subwavelength grating on an $AlO_x$ layer for a vertical-cavity surface-emitting laser," OSA Contin. **3**, 317–324 (2020).
26. J. Zhang and A. Liu, "Dispersion engineering for a metastructure composed of a high-contrast subwavelength grating and a distributed Bragg reflector," Adv. Photon. Res. **2**, 2000172 (2021).
27. J. Zhang, B. Yang, and A. Liu, "Design of 940 nm VCSEL with metastructure," Proc. SPIE **11182**, 111820O (2019).
28. Z. Khan, J.-C. Shih, R.-L. Chao, T.-L. Tsai, H.-C. Wang, G.-W. Fan, Y.-C. Lin, and J.-W. Shi, "High-brightness and high-speed vertical-cavity surface-emitting laser arrays," Optica **7**, 267–275 (2020).
29. M. Agustin, N. Ledentsov, Jr., J.-R. Kropp, V. A. Shchukin, V. P. Kalosha, K. L. Chi, Z. Khan, J. W. Shi, and N. N. Ledentsov, "50 Gb/s NRZ and 4-PAM data transmission over OM5 fiber in the SWDM wavelength range," Proc. SPIE **10552**, 1055202 (2018).
30. G. Larisch, R. Rosales, and D. Bimberg, "Energy-efficient 50+ Gb/s VCSELs for 200+ Gb/s optical interconnects," IEEE J. Sel. Top. Quantum Electron. **25**, 1701105 (2019).
31. T. N. Huynh, F. Doany, D. M. Kuchta, D. Gazula, E. Shaw, J. O'Daniel, and J. Tatum, "4×50 Gb/s NRZ shortwave-wavelength division multiplexing VCSEL link over 50 m multimode fiber," in *Optical Fiber Communication Conference* (2017), paper Tu2B.5.
32. A. Liu, P. Wolf, J.-H. Schulze, and D. Bimberg, "Fabrication and characterization of integrable GaAs-based high-contrast grating reflector and Fabry–Pérot filter array with GaInP sacrificial layer," IEEE Photon. J. **8**, 2700509 (2016).
33. M. C. Y. Huang, Y. Zhou, and C. J. Chang-Hasnain, "Single mode high-contrast subwavelength grating vertical cavity surface emitting lasers," Appl. Phys. Lett. **92**, 171108 (2008).
34. C. Chase, Y. Zhou, and C. J. Chang-Hasnain, "Size effect of high contrast gratings in VCSELs," Opt. Express **17**, 24002–24007 (2009).
35. D. Zhao, Z. Ma, and W. Zhou, "Field penetrations in photonic crystal Fano reflectors," Opt. Express **18**, 14152–14158 (2010).
36. G. C. Park, W. Xue, M. Piels, D. Zibar, J. Mørk, E. Semenova, and I.-S. Chung, "Ultrahigh-speed Si-integrated on-chip laser with tailored dynamic characteristics," Sci. Rep. **6**, 38801 (2016).
37. L. A. Coldren, S. W. Corzine, and M. L. Mašanović, *Diode Lasers and Photonic Integrated Circuits*, 2nd ed. (Wiley, 2012).
38. M. Boroditsky, K. W. Kim, Y. Rahmat-Samii, and E. Yablonovitch, "Smallest possible electromagnetic mode volume in a dielectric cavity," IEE Proc. Optoelectron. **145**, 391–397 (1998).
39. D. M. Kuchta, A. V. Rylyakov, F. E. Doany, C. L. Schow, J. E. Proesel, C. W. Baks, P. Westbergh, J. S. Gustavsson, and A. Larsson, "A 71 Gb/s NRZ modulated 850 nm VCSEL-based optical link," IEEE Photon. Technol. Lett. **27**, 577–580 (2015).
40. J. Lavrencik, S. Varughese, V. A. Thomas, J. S. Gustavsson, E. Haglund, A. Larsson, and S. E. Ralph, "102 Gbps PAM-2 over 50 m OM5 fiber using 850 nm multimode VCSELs," in *IEEE Photonics Conference* (2019), pp. 1–2.